

Infrared-laser-pulse-enhanced ultrafast fragmentation of N_2^{2+} following Auger decay: Mixed quantum-classical simulations

Murali Krishna Ganesa Subramanian,^{1,2,*} Robin Santra,^{1,2,3} and Ralph Welsch¹

¹*Center for Free-Electron Laser Science, DESY, Notkestrasse 85, D-22607 Hamburg, Germany*

²*Department of Physics, University of Hamburg, Jungiusstrasse 9, D-20355 Hamburg, Germany*

³*The Hamburg Centre for Ultrafast Imaging, Luruper Chaussee 149, D-22761 Hamburg, Germany*



(Received 10 August 2018; published 19 December 2018)

We employ mixed quantum-classical molecular dynamics simulations to investigate the fragmentation of N_2 molecules after core-level photoionization by an x-ray laser, subsequent Auger decay, and followed by a femtosecond IR pulse that interacts with N_2^{2+} . The delayed IR pulse couples the dissociative electronic states of N_2^{2+} with electronic states that can support long-lived vibrational resonances. We compare our simulations with previous quantum dynamics calculations in a quasidiabatic representation, which employed a small number of electronic states. Good agreement for both the Auger spectrum as well as the influence of the delayed IR pulse is found. By employing the mixed quantum-classical treatment, we can greatly reduce the computational cost to simulate the fragmentation dynamics compared to the quantum dynamics simulations. Furthermore, we reinvestigate the title process by employing an extended set of adiabatic potential energy surfaces and also investigate the role of nonadiabatic coupling in the process. The use of the full set of adiabatic potentials increases the dissociation probability and changes the details of the interaction with the IR pulse, but no effect due to the nonadiabatic coupling is found.

DOI: [10.1103/PhysRevA.98.063421](https://doi.org/10.1103/PhysRevA.98.063421)

I. INTRODUCTION

The technological advances of x-ray free-electron lasers (FELs) allow the study of complex molecular processes with high temporal and spatial resolution. Pump-probe experiments using FELs give the possibility to observe ultrafast phenomena in quantum systems that occur on the time scale of few tens to hundreds of femtoseconds. In particular, ultrashort x-ray pulses at FELs can be used to track atomic motion in molecules during photochemical processes [1]. Using the Linac Coherent Light Source (LCLS) at SLAC National Laboratory [2] core-shell ionization and subsequent dynamics in diatomic and polyatomic molecules such as N_2 , H_2S , and SF_6 have been investigated [3–6].

Molecular nitrogen and its dication have been well studied in spectroscopy because of their metastable states [7–16]. To investigate the x-ray ionization and subsequent fragmentation dynamics of N_2 , time-resolved pump-probe experiments were performed at LCLS [1]. Following core-shell ionization by an x-ray pulse, molecular N_2^{2+} is produced by Auger decay. The N_2 dication has a few vibrationally long-lived quasibound metastable states [7,17–19]. The experiment observed the unfragmented- N_2^{2+} yield as a function of time delay between the ionizing x-ray pulse and a subsequent IR pulse. A decrease in the unfragmented- N_2^{2+} yield has been reported from the experiment [1].

In a recent quantum dynamics (QD) [20] investigation, the interaction of the IR pulse with the dicationic system

as a function of time delay of the IR pulse has been investigated using the multiconfiguration time-dependent Hartree (MCTDH) [21–23] method and similar trends as in the experiment have been observed [20]. Additionally, the dependence of unfragmented N_2^{2+} on intensity and width of the IR pulse was investigated. For certain Auger energies and pulse delays, a slight increase in the unfragmented- N_2^{2+} yield was found. However, the exact wave packet propagation is very time consuming and its computational cost scales exponentially with increasing system size. Thus, this approach is less suitable to investigate the IR control of Coulomb explosions in polyatomic systems.

This work assesses the prospects of using the computationally efficient Tully's fewest switches surface hopping (FSSH) approach [24–28] to investigate the ultrafast dissociation of N_2^{2+} . In FSSH the electrons are treated quantum mechanically, while the nuclei are treated classically, propagating along a trajectory $R(t)$. The classical trajectories evolve on a single potential energy surface (PES) and can switch between the electronic states based on a hopping probability, which is determined from the nonadiabatic coupling vector and the transition dipole moment for the case of an applied electric field [29–38].

The paper is organized as follows: In Sec. II, the basic expressions underlying the theory and the computational methods used in this work are presented. Section III discusses the Auger spectrum and unfragmented- N_2^{2+} yield, in a quasidiabatic representation from FSSH simulations, and compares to previous QD simulations [20]. Section IV gives a detailed discussion of the fragmentation dynamics in the adiabatic representation in comparison to the dynamics

*Corresponding author: murali.krishna@cfel.de

in the quasidiabatic representation and discusses the impact of nonadiabatic couplings. Finally, Sec. V summarizes this work.

II. THEORETICAL BACKGROUND

A. Fewest switches surface hopping

Throughout this work FSSH [24–27,29–39] is employed and the implementation largely follows Ref. [40]. In FSSH the electrons are treated quantum mechanically, while the nuclei are treated classically, propagating along a trajectory $R(t)$. The classical trajectories evolve on a single PES and can switch between the electronic states based on a hopping probability. To this end, the time-dependent Schrödinger equation (TDSE) for the electrons is solved along the nuclear trajectory,

$$i\hbar\dot{c}_k(t) = \sum_j c_j(t)[V_{kj} - i\hbar\dot{R} \cdot \vec{d}_{kj}], \quad (1)$$

where the c_j are the expansion coefficients with respect to the representation adopted, the V_{kj} are the matrix elements of the electronic Hamiltonian, and the \vec{d}_{kj} are the nonadiabatic coupling vectors (NAC). In the adiabatic representation, the matrix V_{kj} is diagonal. In the following, the adiabatic representation is assumed and, thus, V_{kj} is omitted if $k \neq j$. From Eq. (1) the rate of change of population of the j th electronic state reads

$$\dot{\rho}_{jj} = \sum_{k \neq j} b_{kj}, \quad (2)$$

where

$$b_{kj} = -2\text{Re}[\rho_{jk}\dot{R} \cdot \vec{d}_{kj}], \quad (3)$$

$$\rho_{jk} = c_j c_k^*, \quad (4)$$

and the probability of switching from state j to state k , $P_{j \rightarrow k}$, is obtained as

$$P_{j \rightarrow k} = \frac{-b_{kj}\Delta t}{\rho_{jj}}, \quad (5)$$

where Δt is the time step for the nuclear dynamics. The hopping probability is compared to a uniformly distributed random number ζ , $0 < \zeta < 1$, and a hop occurs if $P_{j \rightarrow k}$ is larger than ζ . If a hop occurs, the velocities of the classical trajectory are adjusted along the direction the nonadiabatic coupling vector to conserve the total energy. Hopping is not performed if there is not enough energy available for this adjustment.

FSSH can be extended to account for coupling of electronic states due to an external field [29–34,36–38,41], where the Hamiltonian for the external field is given by $H_{\text{ext}} = -\vec{E}(t) \cdot \vec{\mu}$, with $\vec{\mu}$ the dipole operator in length form. In this work a Gaussian shaped pulse polarized along the z axis is used and

$$\vec{E}(t) = E_0 e^{-\frac{1}{2}(\frac{t-t_0}{\sigma})^2} \cos(\hbar\omega_f(t-t_0) + \Phi) \hat{z}, \quad (6)$$

where E_0 is the field amplitude, t_0 is the pulse center, σ is the pulse width, $\hbar\omega_f$ is the photon energy, and Φ is the phase of the electric field relative to the Gaussian envelope. The

corresponding TDSE reads

$$i\hbar\dot{c}_k(t) = c_k(t)V_k - i\hbar \sum_j c_j(t)[\dot{R} \cdot \vec{d}_{kj} - i\vec{E}(t) \cdot \vec{\mu}_{kj}], \quad (7)$$

and we obtain the rate of change of population as

$$\dot{\rho}_{jj} = \sum_{k \neq j} -2\text{Re}[\rho_{jk}\dot{R} \cdot \vec{d}_{kj}] + 2\text{Re}[i\rho_{jk}\vec{E}(t) \cdot \vec{\mu}_{kj}]. \quad (8)$$

The probability of hopping is then given as in Eq. (5). However, for this case, the velocity is only adjusted if the hop is due to the nuclear motion and not if the hop is mediated by the electric field as the energy for the hop is transferred to the system by the external field. To decide if a hop is due to the external electric field or due to the nuclear motion, the ratio of the magnitude of the two terms in Eq. (8) is calculated and a Monte Carlo strategy is employed to sample the ratio and to decide on the velocity adjustment.

B. Initial conditions, photoionization, and Auger decay

Initial nuclear positions and velocities on the ground-state PES of N_2 are obtained by either quasiclassical sampling or Wigner sampling of the normal mode coordinate [42,43].

In the quasiclassical sampling, the ensemble of Cartesian positions \mathbf{X} and velocities \mathbf{V} for the classical trajectories are calculated by [43]

$$\mathbf{X}_i = \mathbf{X}_{\text{eq}} + \frac{\mathbf{L}}{\sqrt{M\omega}} \cos(2\pi r_i), \quad (9)$$

$$\mathbf{V}_i = -\frac{\mathbf{L}\sqrt{\omega}}{\sqrt{M}} \sin(2\pi r_i), \quad (10)$$

where $i = 1, \dots, N$ numbers the sample, \mathbf{L} , M , and ω are the normal mode coordinate, normal mode mass, and normal mode frequency, respectively, \mathbf{X}_{eq} is the ground-state equilibrium geometry, and r_i is a uniformly distributed random number in the interval $[0,1]$.

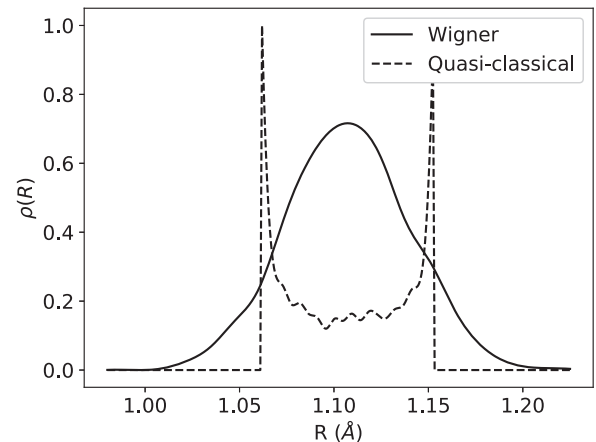


FIG. 1. The distribution of the initial N-N distance obtained from both the Wigner (solid line) and quasiclassical (dashed line) sampling methods.

The Wigner distribution [42] for the vibrational ground state is given as

$$W^{(n=0)}(R, P) = e^{-(P^2+R^2)}, \quad (11)$$

where (R, P) is a point in phase space. The Wigner distribution is sampled employing the von Neumann rejection scheme [42]. The corresponding phase space points are transformed to Cartesian coordinates,

$$\mathbf{X}_i = \mathbf{X}_{eq} + \frac{\mathbf{L}R_i}{\sqrt{M\omega}}, \quad (12)$$

$$\mathbf{V}_i = \frac{\mathbf{L}P_i\sqrt{\omega}}{\sqrt{M}}. \quad (13)$$

Please note that the harmonic approximation is employed in this work for sampling the ground vibrational state of N_2 . The average energy of the initial trajectories is thus $\langle E \rangle = \frac{1}{2}\hbar\omega = 0.14$ eV, which is larger than the exact energy expectation value of 0.12 eV [20], the energy of the wave packet employed in the quantum dynamics calculations [20].

Both sampling methods have certain strengths and weaknesses. On the one hand, the Wigner sampling faithfully reproduces the position distribution of the initial quantum wave packet (see Fig. 1). The quasiclassical sampling, however, results in a distribution that peaks at the classical turning points (see Fig. 1). On the other hand, the quasiclassical sampling reproduces the energy spread of the sampled vibrational ground state, $\Delta E = \sqrt{\langle E^2 \rangle - \langle E \rangle^2} = 0$ eV, while

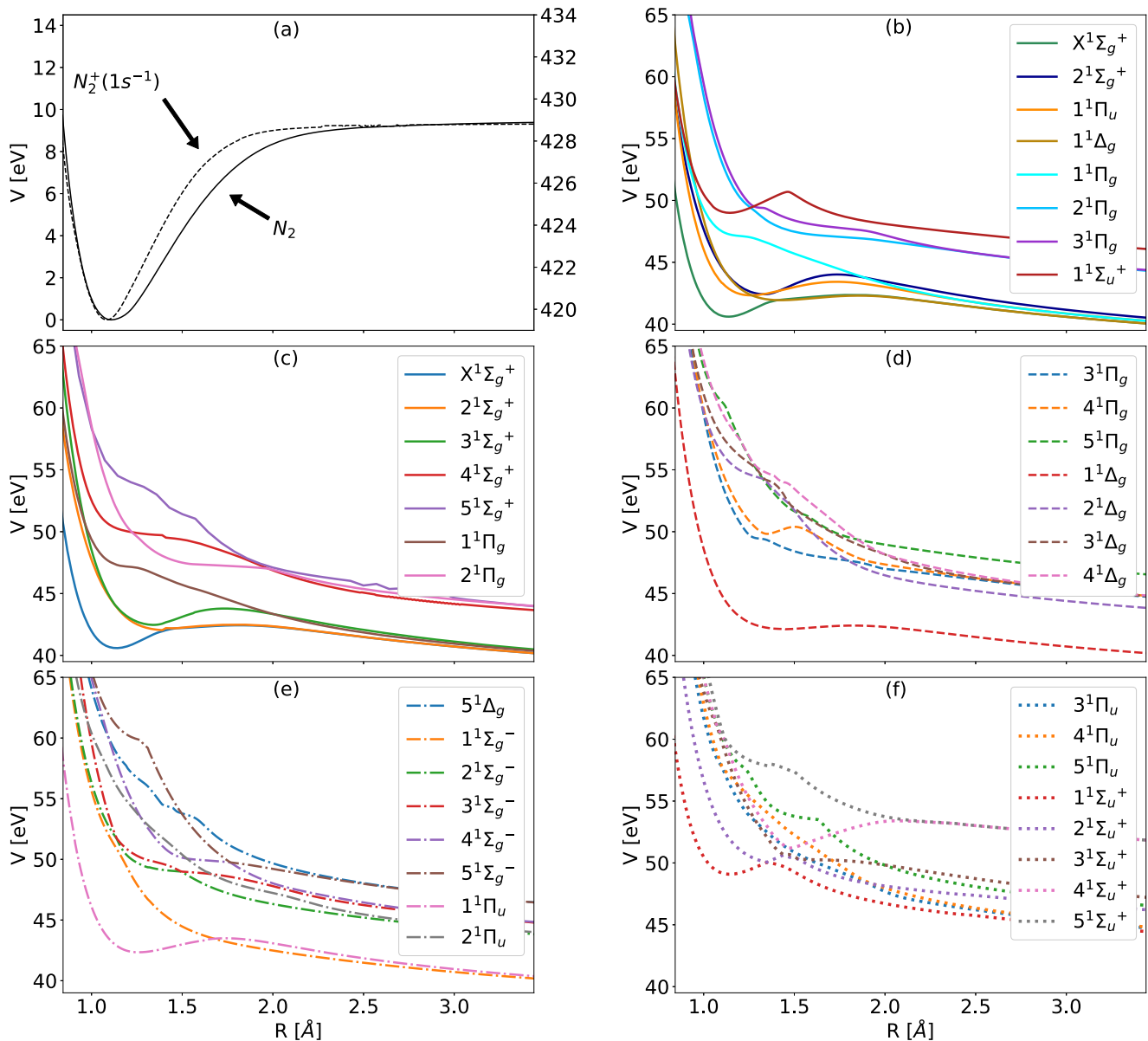


FIG. 2. PESs employed in this work are relative to the ground-state minimum of N_2 . (a) The PES of N_2 (solid line) corresponds to the left-hand side y axis and the PES of core-ionized $N_2^+(1s^{-1})$ (dashed line) corresponds to the right-hand-side y axis. (b) Eight quasiclassical PESs of N_2^{2+} as employed in previous QD simulations [20]. (c)–(f) Thirty adiabatic PESs of N_2^{2+} calculated at the CASSCF/aug-cc-pVTZ level of theory.

the Wigner sampling gives $\Delta E = \frac{1}{2}\hbar\omega = 0.14$ eV for the present case of an initial harmonic state. In this work, we have sampled 5000 trajectories of N_2 molecules that are initially aligned along the z axis. Then a counterclockwise rotation around the y axis with uniformly distributed random angles is performed to mimic the distribution of the rotational ground state relative to the IR polarization axis [20].

The sampled geometries are vertically lifted to the core-ionized N_2^+ electronic state and propagated on that PES. Please note that we follow Ref. [20] and only employ the core-ionized N_2^+ electronic state that corresponds to σ_u symmetry. The N_2^+ electronic state with σ_g symmetry is separated by about 100 meV [16,44] and thus inclusion of this electronic state would only have minimal effect on the results presented. A Monte Carlo scheme is employed to mimic the Auger decay [45,46] and the Auger rates are taken to be the same as in the previous QD simulation [20]. Please note that, following Ref. [20], we assume that the IR pulse has no effect on the Auger decay. If an Auger decay occurs, the trajectory is switched to the corresponding N_2^{2+} state and is subsequently propagated on the manifold of N_2^{2+} electronic states under the influence of the IR pulse as described in Sec. II A.

C. Electronic structure calculations

Electronic structure data such as energies, gradients, nonadiabatic coupling vectors, and transition dipole elements are calculated at the complete active space self-consistent field (CASSCF) level of theory employing the aug-cc-pVTZ basis set developed by Dunning [47] using the MOLCAS 8.2 package [48–51]. The nonadiabatic coupling vector \vec{d}_{kj} is obtained using finite differences as [28]

$$d_{kj} \left(R + \frac{\Delta R}{2} \right) = \frac{1}{2\Delta R} (\langle \phi_k(r; R) | \phi_j(r; R + \Delta R) \rangle - \langle \phi_k(r; R + \Delta R) | \phi_j(r; R) \rangle). \quad (14)$$

All the above mentioned electronic structure quantities are calculated on a regular R grid between 0.5 and 3.5 Å at a spacing of 0.01 Å and then interpolated on-the-fly using the smoothed spline interpolation scheme [52–54] in PYTHON. Figure 2 displays the different PESs employed in this work. Figure 2(a) displays the ground electronic state of N_2 and the core-ionized state of N_2^+ [20]. The two PESs are separated by about 420 eV; however, the minimum of the N_2^+ PES is in the Franck-Condon region. Figure 2(b) displays the quasidiabatic PESs of N_2^{2+} that were used in the previous QD simulations [20]. The $X^1\Sigma_g^+$ and $1^1\Sigma_u^+$ states have a local minimum in the Franck-Condon region. In contrast, the local

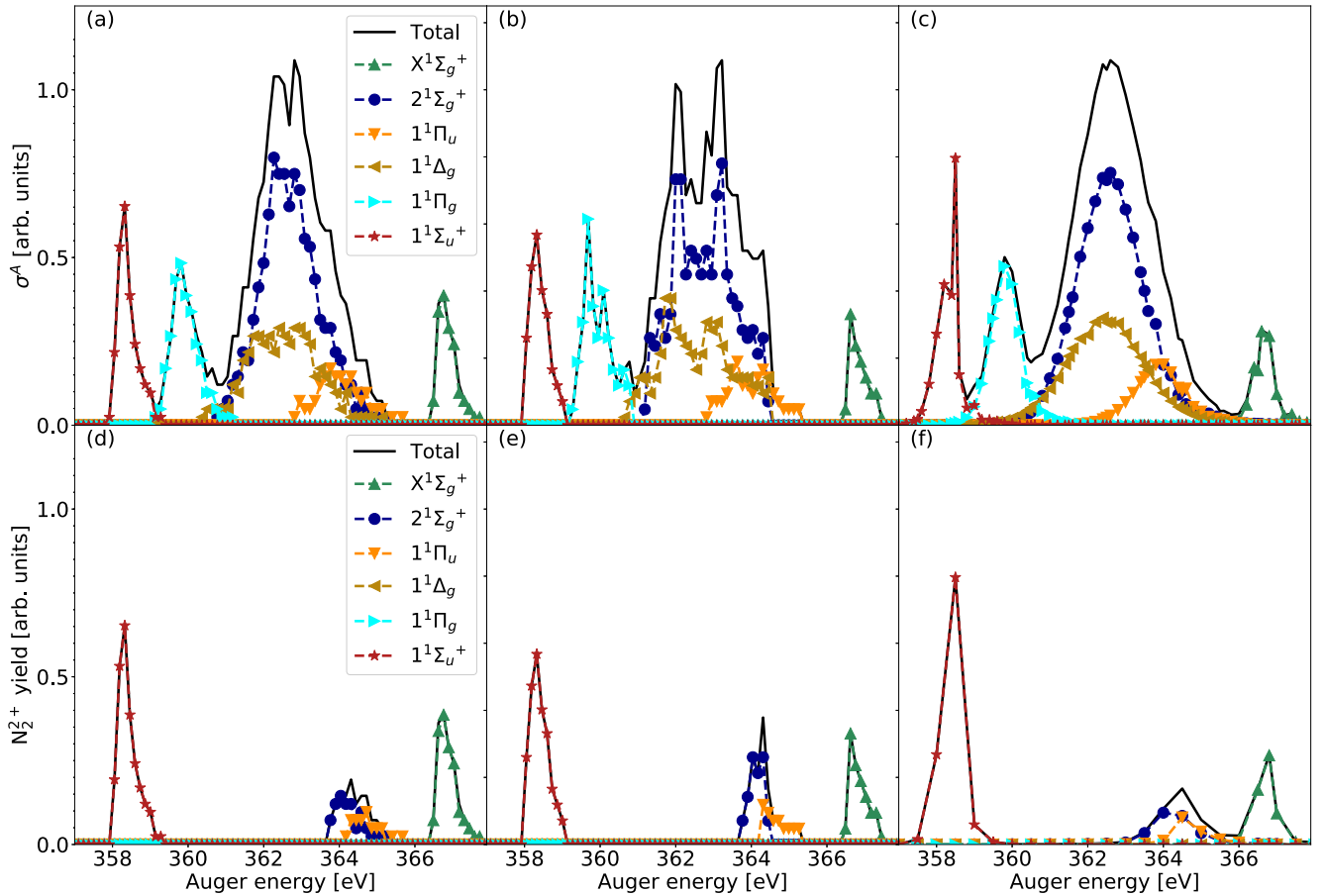


FIG. 3. Auger spectrum using quasidiabatic PESs [shown in Fig. 2(b)] from (a) FSSH (Wigner sampling), (b) FSSH (quasiclassical sampling), and (c) QD [20]. Unfragmented N_2^{2+} (IR free) from (d) FSSH (Wigner sampling), (e) FSSH (quasiclassical sampling), and (f) QD [20].

minima of the $1^1\Delta_g$, $2^1\Sigma_g^+$, and $1^1\Pi_u$ states are located outside of the Franck-Condon region, and the $1^1\Pi_g$, $2^1\Pi_g$, and $3^1\Pi_g$ do not show any local minimum.

Due to the high computational cost of the exact QD simulations, only a small set of quasidiabatic, uncoupled states could be employed in the previous work [20]. As the FSSH simulations performed in this work have a greatly reduced computational cost, we also studied an extended set of 30 adiabatic states of N_2^{2+} in the energy region of interest, which are depicted in Figs. 2(c)–2(f). Additionally, we investigated the role of nonadiabatic coupling in the Coulomb explosion.

III. COMPARISON TO QUANTUM DYNAMICS SIMULATIONS

A. Auger spectrum

In Fig. 3 the Auger electron kinetic-energy spectrum $\sigma^A(E)$ is presented (no IR pulse present). The full Auger spectrum obtained from FSSH employing both Wigner and quasiclassical sampling [Figs. 3(a) and 3(b), respectively] gives very good agreement with previous QD simulations [Fig. 3(c)] [20]. Please note that the Auger spectrum displayed in Fig. 3 is shifted by 11.95 eV, as was done in the QD simulations [20]. The peak positions and the peak widths match the QD spectrum, but small deviations are found for the relative peak heights. The Auger spectrum obtained from quasiclassical sampling shows a small splitting of the peaks, due to the inaccurate initial distribution (see also Fig. 1).

Figures 3(d)–3(f) show the Auger energy dependent unfragmented- N_2^{2+} yield from FSSH employing Wigner sampling (d), quasiclassical sampling (e), and from QD simulations (f) [20]. Very good agreement is found between all three simulations. Auger decay into the $1^1\Pi_g$ state leads to complete dissociation of N_2^{2+} due to its dissociative PES as shown and discussed in Sec. II A. The $1^1\Delta_g$ state has a shallow local minimum away from the Franck-Condon region, which also leads to complete dissociation. The $2^1\Sigma_g^+$ and $1^1\Pi_u$ states lead to partial dissociation. The local minimum on each PES

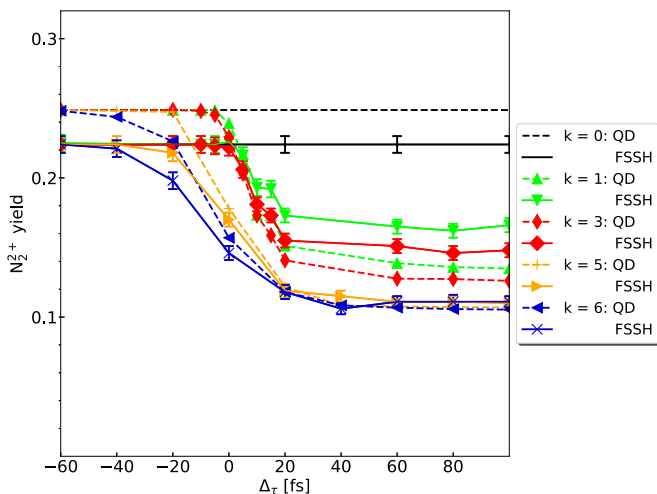


FIG. 4. N_2^{2+} yield from FSSH (solid lines) and QD (dashed lines) in the presence of IR pulses with the pulse parameters given in Table I.

TABLE I. Parameters for the IR pulses employed in this work (cf. Ref. [20]).

IR pulse	I_0 (10^{14} W cm^{-2})	Δ_{IR} (FWHM) (fs)
$k = 0$	–	–
$k = 1$	6.68	3.54
$k = 3$	3.37	7.07
$k = 5$	0.84	28.28
$k = 6$	0.56	42.43

has a considerable depth, but both minima are away from the Franck-Condon region. The overall N_2^{2+} yield from the FSSH calculation is 0.22, which is slightly lower than the value obtained from QD simulations, which is 0.25 [20]. This difference is due to the initial energy of the trajectories, which is greater than the initial energy of the QD wave packet as discussed in Sec. II B. The results obtained with the Wigner sampling resemble the QD results slightly better due to the faithful reproduction of the initial quantum distribution. Thus,

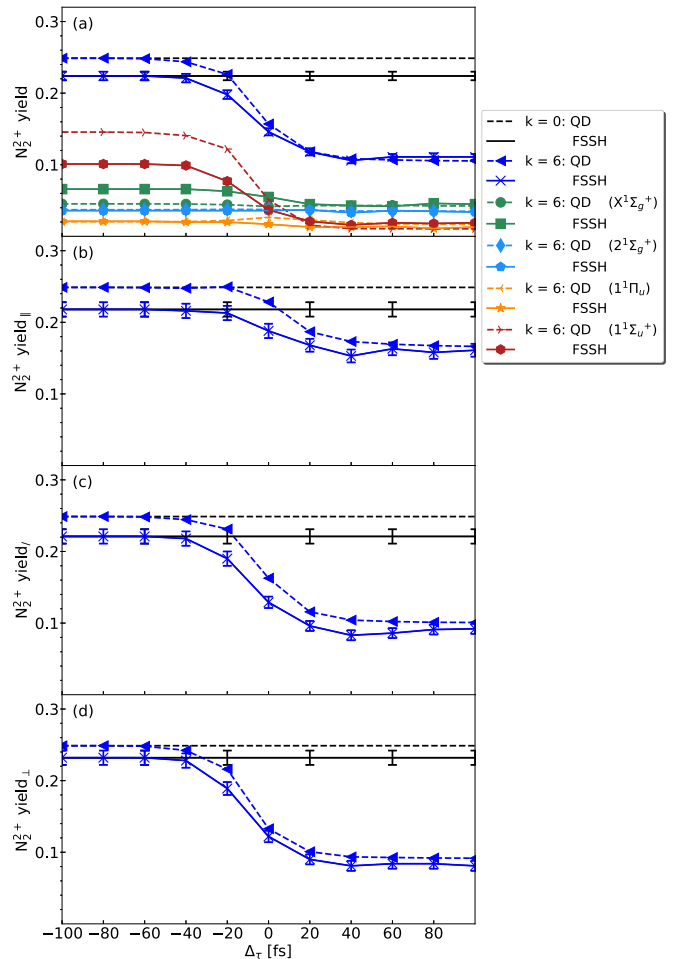


FIG. 5. N_2^{2+} yield with ($k = 6$) and without ($k = 0$) IR pulse. FSSH results are given by solid lines and QD results are given by dashed lines. (a) Overall N_2^{2+} yield as well as contributions from different Auger channels. (b) and (c) N_2^{2+} yield for alignment of N_2 parallel, diagonal, and perpendicular to the IR field.

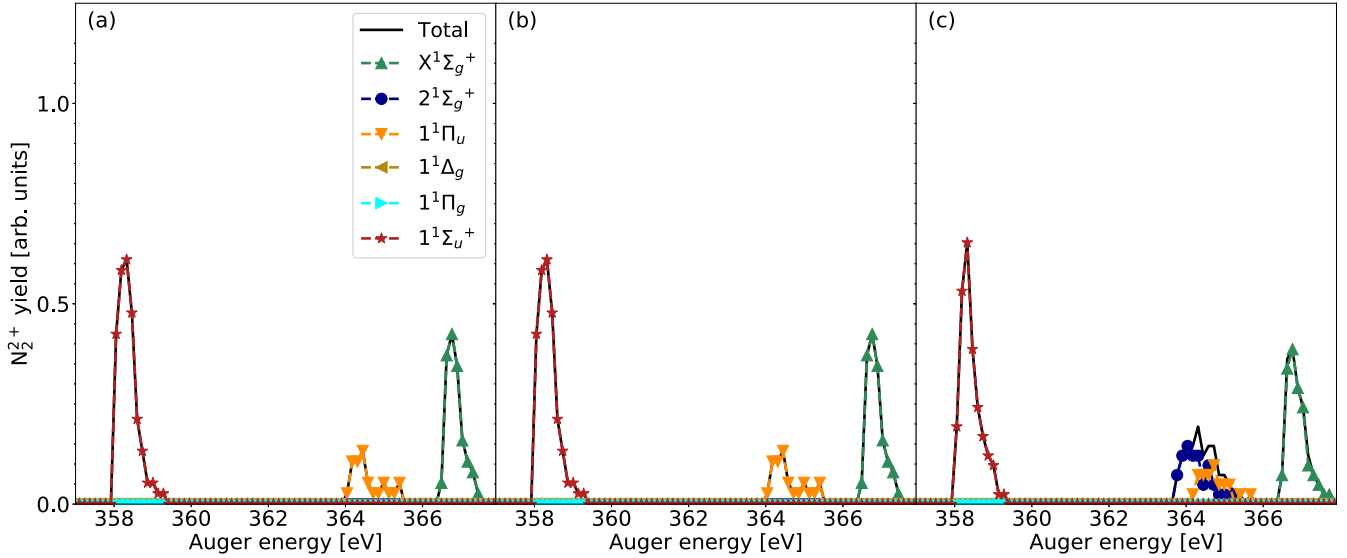


FIG. 6. N_2^{2+} yield (IR free) as a function of energy using the adiabatic PESs [shown in Figs. 2(c)–2(f)] from (a) FSSH (without NAC) and (b) FSSH (with NAC) in comparison to the N_2^{2+} yield from (c) FSSH using quasidiabatic PESs [same as in Fig. 3(d)].

for the remainder of this paper, we will show only results obtained with the Wigner sampling.

B. N_2^{2+} yield in the presence of an IR pulse

Figure 4 shows the unfragmented- N_2^{2+} yield from FSSH (solid lines) and QD [20] (dashed lines) as a function of time delay of an IR pulse, where the parameters of the different IR pulses are given in Table I. As discussed in the previous section (Sec. III A), the IR free ($k = 0$) yield obtained from FSSH is slightly smaller than the yield obtained from QD [20] due to the approximations in the initial sampling. In the presence of long IR pulses ($k = 5$ and $k = 6$), the unfragmented- N_2^{2+} yield from FSSH shows very good agreement with QD [20]. For short IR pulses ($k = 1$ and $k = 3$), we found less N_2^{2+} fragmentation from FSSH than QD [20]. This difference can be rationalized by the approximations in the sampling of the initial conditions. In particular, due to the harmonic approximation, the initial distribution is symmetric as compared to the slightly asymmetric initial distribution of the exact ground state in the QD simulations and the initial energy of the trajectories is slightly overestimated in FSSH. Additionally, the sampling of initial conditions ignores any rovibrational coupling, which is present in the QD simulations. Small differences in the dynamics resulting from the approximations in the sampling manifest themselves more strongly for short IR pulses than long IR pulses, due to less averaging in the former case. These shortcomings could, for example, be overcome by employing the ring polymer molecular dynamics approach [55,56] with nonequilibrium initial conditions [57] and surface hopping [58,59]. This is left for future work.

Figure 5 shows the unfragmented- N_2^{2+} yield as a function of time delay for the long IR pulse ($k = 6$) and no IR pulse ($k = 0$). Figure 5(a) gives the total yield of unfragmented- N_2^{2+} , which we discussed in the previous paragraph. The total unfragmented- N_2^{2+} yield in the presence of a long IR pulse ($k = 6$) shows very good agreement with QD simulations [20].

Figure 5(a) also gives the N_2^{2+} yield from the individual Auger channels. Again good agreement between the FSSH and QD simulations is found. The largest differences can be found for IR free cases (i.e., very negative delay times), which have been discussed above (cf. Fig. 3). In the presence of an IR pulse very good agreement between FSSH and QD simulations is found. The $2^1\Sigma_g^+$ channel does not undergo any fragmentation and $1^1\Pi_u$ undergoes minimal dissociation. The same behavior was observed in the QD simulations [20].

Figures 5(b)–5(d) show the N_2^{2+} yield for different initial alignments of the N_2 molecular axis relative to the IR polarization axis given by an angle θ . To this end, we define three regions: parallel (yield $_{\parallel}$) to the field ($0^\circ < \theta < 30^\circ$ and $150^\circ < \theta < 180^\circ$), diagonal (yield $_{\diag}$) to the field ($30^\circ < \theta < 60^\circ$ and $120^\circ < \theta < 150^\circ$), and perpendicular (yield $_{\perp}$) to the field ($60^\circ < \theta < 120^\circ$) [20]. All these quantities show good agreement with the QD simulations. The reduced computational cost and better scaling of FSSH compared to QD, while giving overall good agreement, will allow for the investigation of bigger systems and more complex dynamics.

IV. FRAGMENTATION IN ADIABATIC REPRESENTATION

Due to the increased efficiency of the FSSH simulations compared to the QD, we can also investigate the fragmentation dynamics including all 30 adiabatic PESs shown in Figs. 2(c)–2(f). In this section, we also investigate the role of non-Born-Oppenheimer effects due to nonadiabatic coupling of these PESs, which could not be done in the QD simulations [20].

Figure 6 shows the N_2^{2+} yield (IR free) as a function of Auger energy for uncoupled ($\vec{d}_{kj} = 0$) adiabatic PESs [Fig. 6(a)] and coupled adiabatic PESs [Fig. 6(b)] in comparison with the previously discussed results on the quasidiabatic PESs [Fig. 6(c)]. We observe that the state $2^1\Sigma_g^+$ leads to complete dissociation of N_2^{2+} compared to partial dissociation for the quasidiabatic PESs. The difference in fragmentation

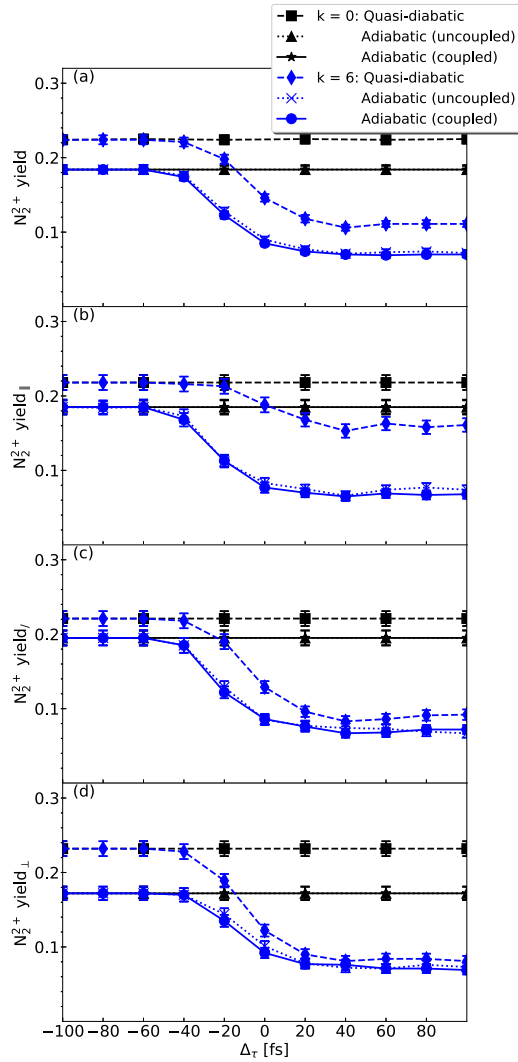


FIG. 7. N_2^{2+} yield from FSSH simulations using quasidiabatic (dashed), uncoupled adiabatic (dotted), and coupled adiabatic (solid) representations. (a) Total N_2^{2+} yield; (b)–(d) N_2 parallel, diagonal, and perpendicular to the IR field.

is due to the higher dissociation barrier on the quasidiabatic PESs, which results from smoothly changing from one to another adiabatic PES when constructing the quasidiabatic PESs and ignoring all off-diagonal potential matrix elements. No difference between the simulations employing uncoupled or fully coupled adiabatic PESs is observed. All other features in the Auger energy dependent IR free N_2^{2+} yield are the same for the adiabatic and quasidiabatic PESs as both sets are similar in the Franck-Condon region.

The increased number of PESs in the simulations that employ the adiabatic representation allows for more possible ways for the IR pulse to excite the system. Therefore, we will now analyze the N_2^{2+} yield when applying an IR pulse. Figure 7 shows the unfragmented- N_2^{2+} yield as a function of time delay of the IR pulse for uncoupled adiabatic (dotted lines) and coupled adiabatic PESs (solid lines) from FSSH simulations in comparison to the previously discussed yield on the quasidiabatic PESs (cf. Fig. 5). The total N_2^{2+} yield is shown in Fig. 7(a). We observe that the IR free N_2^{2+}

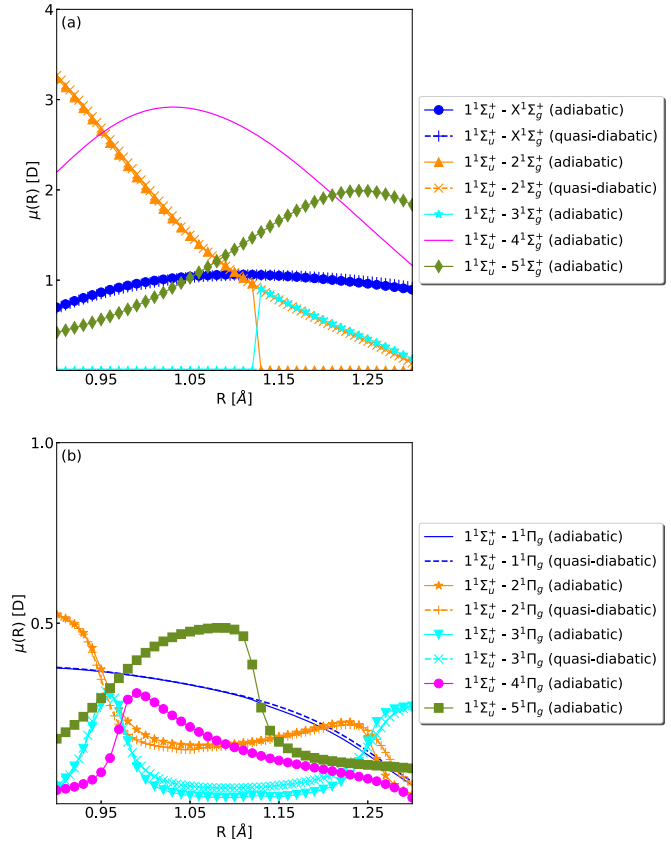


FIG. 8. Magnitude of (a) parallel (z) and (b) perpendicular (x, y) components of the transition dipole moments (μ) of the dominant metastable state $1^1\Sigma_u^+$ in the Franck-Condon region.

yield employing the adiabatic PESs (both coupled and uncoupled) is lower than on the quasidiabatic PESs, as discussed above (cf. Fig. 6). Overall, a similar magnitude of dissociation due to the IR pulse is found for the adiabatic and quasidiabatic PESs. No impact of nonadiabatic coupling is found for the cases considered in this work.

Figures 7(b)–7(d) give the unfragmented- N_2^{2+} yield in the three different alignment regions discussed in Sec. III B. In the presence of the IR pulse, we observe a different N_2^{2+} yield in these regions (coupled and uncoupled PESs) compared to the quasidiabatic PESs. This effect is most pronounced for N_2 aligned parallel to the IR field. This difference can be attributed to the inclusion of more adiabatic PESs, which gives trajectories the possibility to hop to more different PESs compared to the previous calculations. This is exemplified for the dominant metastable state $1^1\Sigma_u^+$. Figure 8 shows the parallel and perpendicular components of the transition dipole moment of $1^1\Sigma_u^+$ with respect to the IR pulse polarization. In the previous simulations this state was optically coupled via the parallel component of the transition dipole moment to two other states (i.e., $X^1\Sigma_g^+$ and $2^1\Sigma_g^+$) in the Franck-Condon region. In contrast, in the extended adiabatic representation, the same state is optically coupled to five other states (i.e., $X^1\Sigma_g^+$, $2^1\Sigma_g^+$, $3^1\Sigma_g^+$, $4^1\Sigma_g^+$, and $5^1\Sigma_g^+$) via the parallel component of the transition dipole moment in the Franck-Condon region. The states $4^1\Sigma_g^+$ and $5^1\Sigma_g^+$ in the adiabatic representation

are strongly coupled with the metastable state $1^1\Sigma_u^+$ via the parallel component [Fig. 8(a)], which results in increased N_2^{2+} fragmentation when the system is parallel to the IR pulse. Similarly, the same state was optically coupled to three other states (i.e., $1^1\Pi_g$, $2^1\Pi_g$, and $3^1\Pi_g$) via the perpendicular component of the transition dipole in the previous simulations. However, in the extended adiabatic representation, it is coupled to five other states (i.e., $1^1\Pi_g$, $2^1\Pi_g$, $3^1\Pi_g$, $4^1\Pi_g$, and $5^1\Pi_g$). Unlike the parallel component, the states $4^1\Pi_g$ and $5^1\Pi_g$ do not have a strong optical coupling via the perpendicular component of the transition dipole moment [Fig. 8(b)]. Thus, the effect of additional states is less strong when the system is diagonal or perpendicular to the IR pulse. Additionally, omitting the quasidiabatic representation and switching to a fully adiabatic representation also changes the coupling pattern. Similar trends are observed also for the other states.

V. CONCLUSION

We have performed x-ray pump-IR probe FSSH simulations of N_2 molecules and compared the results with previous QD simulations [20]. The x-ray pulse photoionizes the N_2 by removing an inner shell electron followed by Auger decay of the N_2^+ system to N_2^{2+} . The interaction of N_2^{2+} with a subsequent IR pulse has been studied. First, we conducted this study in the quasidiabatic (eight N_2^{2+} states) representation employed in the previous QD [20] studies. Results from FSSH

simulations for long IR pulses are in good agreement with the QD simulations [20], whereas we observe slightly less fragmentation of N_2^{2+} in the presence of short IR pulses. This can be rationalized by the approximations made for sampling the initial conditions. Due to the increased efficiency of the FSSH simulations, we could reinvestigate the problem employing an extended set of 30 adiabatic PESs. In the adiabatic representation, the total unfragmented- N_2^{2+} yield is decreased compared to simulations in the quasidiabatic representation. Moreover, in contrast to the conclusions of Ref. [20], we find IR-induced molecular fragmentation for parallel alignment to be as strong as for perpendicular alignment. No impact of nonadiabatic coupling is found. FSSH greatly reduced the simulation cost and has a better scaling than QD simulations [20], which opens the door for investigation of fragmentation dynamics for larger systems. Polyatomic systems can be treated in mixed quantum-classical simulations by either on-the-fly electronic structure calculations or by using fitted PES, e.g., employing machine learning techniques.

ACKNOWLEDGMENTS

We thank Athiya Mahmud Hanna for the fruitful discussions. This work has been supported financially by the Deutsche Forschungsgemeinschaft (DFG) within the framework of the SFB 925 “Light-induced dynamics and control of correlated quantum systems.”

-
- [1] J. M. Glowonia, J. Cryan, J. Andreasson, A. Belkacem, N. Berrah, C. I. Blaga, C. Bostedt, J. Bozek, L. F. DiMauro, L. Fang, J. Frisch, O. Gessner, M. Gühr, J. Hajdu, M. P. Hertlein, M. Hoener, G. Huang, O. Kornilov, J. P. Marangos, A. M. March, B. K. McFarland, H. Merdji, V. S. Petrovic, C. Raman, D. Ray, D. A. Reis, M. Trigo, J. L. White, W. White, R. Wilcox, L. Young, R. N. Coffee, and P. H. Bucksbaum, *Opt. Express* **18**, 17620 (2010).
- [2] P. Emma, R. Akre, J. Arthur, R. Bionta, C. Bostedt, J. Bozek, A. Brachmann, P. Bucksbaum, R. Coffee, F.-J. Decker, Y. Ding, D. Dowell, S. Edstrom, A. Fisher, J. Frisch, S. Gilevich, J. Hastings, G. Hays, P. Hering, Z. Huang, R. Iverson, H. Loos, M. Messerschmidt, A. Miahnahri, S. Moeller, H.-D. Nuhn, G. Pile, D. Ratner, J. Rzepiela, D. Schultz, T. Smith, P. Stefan, H. Tompkins, J. Turner, J. Welch, W. White, J. Wu, G. Yocky, and J. Galayda, *Nat. Photon.* **4**, 641 (2010).
- [3] N. Berrah, L. Fang, T. Osipov, B. Murphy, C. Bostedt, and J. D. Bozek, *J. Electron. Spectrosc. Relat. Phenom.* **196**, 34 (2014).
- [4] T. Osipov, L. Fang, B. Murphy, F. Tarantelli, E. R. Hosler, E. Kukk, J. D. Bozek, C. Bostedt, E. P. Kanter, and N. Berrah, *J. Phys. B: At., Mol. Opt. Phys.* **46**, 164032 (2013).
- [5] B. F. Murphy, L. Fang, M.-H. Chen, J. D. Bozek, E. Kukk, E. P. Kanter, M. Messerschmidt, T. Osipov, and N. Berrah, *Phys. Rev. A* **86**, 053423 (2012).
- [6] L. Fang, T. Osipov, B. Murphy, F. Tarantelli, E. Kukk, J. P. Cryan, M. Glowonia, P. H. Bucksbaum, R. N. Coffee, M. Chen, C. Buth, and N. Berrah, *Phys. Rev. Lett.* **109**, 263001 (2012).
- [7] R. W. Wetmore and R. K. Boyd, *J. Phys. Chem.* **90**, 5540 (1986).
- [8] P. R. Taylor and H. Partridge, *J. Phys. Chem.* **91**, 6148 (1987).
- [9] B. Kempgens, A. Kivimäki, M. Neeb, H. M. Köppe, A. M. Bradshaw, and J. Feldhaus, *J. Phys. B: At. Mol. Opt. Phys.* **29**, 5389 (1996).
- [10] W. Jiang, Y. G. Khait, and M. R. Hoffmann, *J. Chem. Phys.* **127**, 164308 (2007).
- [11] J. P. Cryan, J. M. Glowonia, J. Andreasson, A. Belkacem, N. Berrah, C. I. Blaga, C. Bostedt, J. Bozek, N. A. Cherepkov, L. F. DiMauro, L. Fang, O. Gessner, M. Gühr, J. Hajdu, M. P. Hertlein, M. Hoener, O. Kornilov, J. P. Marangos, A. M. March, B. K. McFarland, H. Merdji, M. Messerschmidt, V. S. Petrović, C. Raman, D. Ray, D. A. Reis, S. K. Semenov, M. Trigo, J. L. White, W. White, L. Young, P. H. Bucksbaum, and R. N. Coffee, *J. Phys. B: At. Mol. Opt. Phys.* **45**, 055601 (2012).
- [12] H. Ågren, *J. Chem. Phys.* **75**, 1267 (1981).
- [13] W. E. Moddeman, T. A. Carlson, M. O. Krause, B. P. Pullen, W. E. Bull, and G. K. Schweitzer, *J. Chem. Phys.* **55**, 2317 (1971).
- [14] S. Svensson, A. N. de Brito, M. P. Keane, N. Correia, L. Karlsson, C. M. Liegener, and H. Agren, *J. Phys. B: At. Mol. Opt. Phys.* **25**, 135 (1992).
- [15] G. Víkor, S. Ricz, L. Tóth, B. Sulik, J. Véghe, Á. Kövér, and L. Kövér, *Nucl. Instrum. Methods Phys. Res. B* **124**, 393 (1997).
- [16] S. Sorensen, C. Miron, R. Feifel, M. N. Piancastelli, O. Björneholm, and S. Svensson, *Chem. Phys. Lett.* **456**, 1 (2008).
- [17] Y. H. Jiang, A. Rudenko, M. Kurka, K. U. Kühnel, T. Ergler, L. Foucar, M. Schöffler, S. Schössler, T. Havermeier, M. Smolarski, K. Cole, R. Dörner, S. Düsterer, R. Treusch, M.

- Gensch, C. D. Schröter, R. Moshhammer, and J. Ullrich, *Phys. Rev. Lett.* **102**, 123002 (2009).
- [18] E. Gagnon, P. Ranitovic, X.-M. Tong, C. L. Cocke, M. M. Murnane, H. C. Kapteyn, and A. S. Sandhu, *Science* **317**, 1374 (2007).
- [19] P. Franceschi, D. Ascenzi, P. Tosi, R. Thissen, J. Žabka, J. Roithová, C. L. Ricketts, M. D. Simone, and M. Coreno, *J. Chem. Phys.* **126**, 134310 (2007).
- [20] A. M. Hanna, O. Vendrell, A. Ourmazd, and R. Santra, *Phys. Rev. A* **95**, 043419 (2017).
- [21] H.-D. Meyer, U. Manthe, and L. Cederbaum, *Chem. Phys. Lett.* **165**, 73 (1990).
- [22] M. Beck, A. Jäckle, G. Worth, and H.-D. Meyer, *Phys. Rep.* **324**, 1 (2000).
- [23] H.-D. Meyer and G. A. Worth, *Theor. Chem. Acc.* **109**, 251 (2003).
- [24] J. C. Tully, *J. Chem. Phys.* **93**, 1061 (1990).
- [25] J. C. Tully, *Int. J. Quantum Chem.* **40**, 299 (1991).
- [26] J. C. Tully, *Faraday Discuss.* **110**, 407 (1998).
- [27] N. Doltsinis and D. Marx, *J. Theor. Comput. Chem.* **1**, 319 (2002).
- [28] E. Fabiano, T. Keal, and W. Thiel, *Chem. Phys.* **349**, 334 (2008).
- [29] G. Granucci and M. Persico, *J. Chem. Phys.* **126**, 134114 (2007).
- [30] G. Granucci, M. Persico, and A. Zocante, *J. Chem. Phys.* **133**, 134111 (2010).
- [31] J. J. Bajo, G. Granucci, and M. Persico, *J. Chem. Phys.* **140**, 044113 (2014).
- [32] J. Petersen and R. Mitrić, *Phys. Chem. Chem. Phys.* **14**, 8299 (2012).
- [33] R. Mitrić, J. Petersen, and V. Bonačić-Koutecký, *Phys. Rev. A* **79**, 053416 (2009).
- [34] G. Tomasello, M. Wohlgemuth, J. Petersen, and R. Mitrić, *J. Phys. Chem. B* **116**, 8762 (2012).
- [35] J. Petersen, M. Wohlgemuth, B. Sellner, V. Bonačić-Koutecký, H. Lischka, and R. Mitrić, *Phys. Chem. Chem. Phys.* **14**, 4687 (2012).
- [36] P. Marquetand, M. Richter, J. González-Vázquez, I. Sola, and L. González, *Faraday Discuss.* **153**, 261 (2011).
- [37] J. J. Bajo, J. González-Vázquez, I. R. Sola, J. Santamaria, M. Richter, P. Marquetand, and L. González, *J. Phys. Chem. A* **116**, 2800 (2012).
- [38] D. Geißler, P. Marquetand, J. González-Vázquez, L. González, T. Rozgonyi, and T. Weinacht, *J. Phys. Chem. A* **116**, 11434 (2012).
- [39] M. E.-A. Madjet, Z. Li, and O. Vendrell, *J. Chem. Phys.* **138**, 094311 (2013).
- [40] S. Bazzi, R. Welsch, O. Vendrell, and R. Santra, *J. Phys. Chem. A* **122**, 1004 (2018).
- [41] F. Agostini, A. Abedi, and E. K. U. Gross, *J. Chem. Phys.* **141**, 214101 (2014).
- [42] L. Sun and W. L. Hase, *J. Chem. Phys.* **133**, 044313 (2010).
- [43] W. L. Hase and D. G. Buckowski, *Chem. Phys. Lett.* **74**, 284 (1980).
- [44] U. Hergenhahn, O. Kugeler, A. Rüdél, E. E. Rennie, and A. M. Bradshaw, *J. Phys. Chem. A* **105**, 5704 (2001).
- [45] Y. Hao, L. Inhester, K. Hanasaki, S.-K. Son, and R. Santra, *Struct. Dyn.* **2**, 041707 (2015).
- [46] S.-K. Son and R. Santra, *Phys. Rev. A* **85**, 063415 (2012).
- [47] J. T. H. Dunning, *J. Chem. Phys.* **90**, 1007 (1989).
- [48] G. Karlström, R. Lindh, P.-Å. Malmqvist, B. O. Roos, U. Ryde, V. Veryazov, P.-O. Widmark, M. Cossi, B. Schimmelpfennig, P. Neogrády, and L. Seijo, *Comput. Mater. Sci.* **28**, 222 (2003).
- [49] V. Veryazov, P.-O. Widmark, L. Serrano-Andres, R. Lindh, and B. Roos, *Int. J. Quantum Chem.* **100**, 626 (2004).
- [50] F. Aquilante, L. D. Vico, N. Ferré, G. Ghigo, P.-Å. Malmqvist, P. Neogrády, T. Pedersen, M. Pitonák, M. Reiher, B. Roos, L. Serrano-Andrés, M. Urban, V. Veryazov, and R. Lindh, *J. Comput. Chem.* **31**, 224 (2010).
- [51] F. Aquilante, J. Autschbach, R. K. Carlson, L. F. Chibotaru, M. G. Delcey, L. D. Vico, I. F. Galván, N. Ferré, L. M. Frutos, L. Gagliardi, M. Garavelli, A. Giussani, C. E. Hoyer, G. L. Manni, H. Lischka, D. Ma, P. Å. Malmqvist, T. Müller, A. Nenov, M. Olivucci, T. B. Pedersen, D. Peng, F. Plasser, B. Pritchard, M. Reiher, I. Rivalta, I. Schapiro, J. Segarra-Martí, M. Stenrup, D. G. Truhlar, L. Ungur, A. Valentini, S. Vancoillie, V. Veryazov, V. P. Vysotskiy, O. Weingart, F. Zapata, and R. Lindh, *J. Comput. Chem.* **37**, 506 (2016).
- [52] C. de Boor, *J. Approx. Theory* **6**, 50 (1972).
- [53] M. G. Cox, *J. Inst. Maths Applics* **10**, 134 (1972).
- [54] P. Dierckx, *Monographs on Numerical Analysis* (Oxford University Press, Oxford, 1995).
- [55] I. R. Craig and D. E. Manolopoulos, *J. Chem. Phys.* **121**, 3368 (2004).
- [56] S. Habershon, D. E. Manolopoulos, T. E. Markland, and T. F. Miller, *Annu. Rev. Phys. Chem.* **64**, 387 (2013).
- [57] R. Welsch, K. Song, Q. Shi, S. C. Althorpe, and T. F. Miller, *J. Chem. Phys.* **145**, 204118 (2016).
- [58] P. Shushkov, R. Li, and J. C. Tully, *J. Chem. Phys.* **137**, 22A549 (2012).
- [59] R. Kaur and R. Welsch (unpublished).